Probing dark matter in 2HDM+S with MeerKAT

N Lavis and G Beck

School of Physics, University of the Witwatersrand,Private Bag 3, WITS-2050, Johannesburg,South Africa

E-mail: 1603551@students.wits.ac.za, geoffrey.beck@wits.ac.za

Abstract. The unknown nature of dark matter remains an eyesore on our cosmological paradigm. Much of the previous work done to probe its properties have used gamma-ray studies, but the impressive sensitivities of new radio instruments are allowing them to become the frontrunners in dark matter searches. MeerKAT is the best instrument of its kind in the southern hemisphere, making it a prime candidate for dark matter indirect hunts. By measuring diffuse synchrotron emission within galaxy clusters observed in the MeerKAT Galaxy Cluster Legacy Survey (MGCLS) we are able to probe the properties of a dark matter model. In this work the 2HDM+S model as well as a sample of generic WIMP channels are considered. The former was developed to explain various anomalies observed in Large Hadron Collider (LHC) data from runs 1 and 2. The use of public MeerKAT data allows us to present some of the first WIMP dark matter constraints produced using this instrument.

1. Introduction

While indirect evidences such as gravitational lensing, galactic rotation curves, and anisotropies in the CMB indicate the presence of dark matter in our Universe, its composition remains unknown. Candidates take many forms, with one of the current favoured forms being WIMPS. For a review of evidences and candidates see Bertone et al. [1]. Methods of investigation include collider searches, attempted direct detections and indirect searches via decay/annihilation products. This work utilizes the latter. The two-Higgs doublet model with an additional singlet scaler (2HDM+S) is a beyond standard model hypothesis that contains a hidden sector dark matter candidate. The model was proposed as an explanation for various anomalies observed in Large Hadron Collider data from runs 1 and 2 [2, 3]. The conjectured mass range of this candidate overlaps with that of astrophysically motivated dark matter models for the PAMELA [4] anti-particle excesses and gamma-ray excesses observed by Fermi-LAT [5] at the galactic centre. In prior indirect dark matter searches gamma-ray experiments, such as Fermi-LAT [6] and HESS [7], have taken preference. This is due to their low attenuation and high detection efficiency. With the introduction of new highly capable radio interferometers such as MeerKAT, the precursor to the SKA, radio frequency dark matter searches are expected to gain prevalence, as there are indications that radio data analysis is an effective method for producing dark matter constraints [8]. The superior angular resolution of such instruments limits confusion between diffuse emission and point sources. By the comparison of measured diffuse synchrotron emission in galaxies from the MeerKAT Galaxy Cluster Legacy Survey (MGCLS) [9] to the predictions produced by modelling the dark matter annihilation within the cluster environments we are able to produce limits for the annihilation cross sections of various annihilation channels for a range of masses.

In this work we extend the results presented in [10] by considering five additional clusters and producing the statistically stacked results of the annihilation cross section upper limits produced with the results of all twelve clusters. These proceedings are structured as follows: Section 2 briefly discusses the 2HDM+S formalism and the dark matter sector it introduces. Section 3 introduces the synchrotron emission formalism with which the simulations are performed. Section 4 introduces MGCLS and the potential benefits of MeerKAT. In section 5 we present and discuss our results.

2. 2HDM+S and Dark Matter

Numerous multi-lepton anomalies have been observed in both run 1 and 2 data from the LHC [2] [3] since the discovery of the Higgs boson [11, 12, 13, 14]. An analysis of the multi-lepton final states indicates a deviation from the Standard Model (SM) predictions. This alludes to the existence of physics beyond the SM. One implication of the 2HDM+S model is the production of multiple leptons via its decay chain H $\rightarrow$ Sh, SS [3]. The heavy Higgs H and scalar boson S have masses fixed to $m_H = 270$ GeV and $m_S = 150$ GeV respectively [15] within the model. There have been statistically compelling excesses reported for opposite and same sign di-leptons as well as the three lepton channel both with and without the presence of b-tagged jets [16] [17] [18]. In addition, evidence for the production of the scalar S with mass 151 GeV was obtained by combining side band data from SM Higgs searches [19]. When all decay channels are included a global significance of 4.8 σ was reported for the required mass range (130 -160 GeV) to explain the anomalies [19]. This validates some of the assumptions within the model. The scalar S can potentially act as a mediator between SM particles and the dark matter candidate that is introduced within the hidden sector of the model.

3. Synchrotron emission model

The formalism for predicting the surface brightness of synchrotron emission within a given halo environment is outlined by Beck et al in [20]. The power of synchrotron emission produced by an electron of energy E within a magnetic field of strength B is given by [21] as:

$$P_{\rm sync}(\nu, E, r, z) = \int_0^{\pi} d\theta \frac{\sin^2\theta}{2} 2\pi\sqrt{3} r_{\rm e} m_{\rm e} c \nu_{\rm g} F_{\rm sync}(\frac{\kappa}{\sin\theta}) \tag{1}$$

where ν is the observed frequency, z is the redshift of the source, $m_{\rm e}$ is the mass of an electron, $\nu_{\rm g} = \frac{cB}{2\pi m_{\rm e} c}$ is the non-relativistic gyro-frequency and $r_{\rm e} = \frac{e^2}{m_{\rm e} c^2}$ is the classical radius of an electron [20].

The parameter κ is defined as

$$\kappa = \frac{2\nu(1+z)}{3\nu_0\gamma}\left(1 + \left(\frac{\nu_{\rm p}\gamma}{\nu(1+z)}\right)^2\right)^{3/2} \tag{2}$$

where ν_p is the plasma frequency, which is directly dependent on the electron density of the environment. The parameter $F_{\rm sync}$ describes the synchrotron kernel and is defined as

$$F_{\rm sync}(x) = x\int_x^{\infty} dy K_{5/3}(y) \approx 1.25 x^{1/3} e^{-x}(648 + x^2)^{1/12} \tag{3}$$

The synchrotron emissivity at a radial position r within a halo is then found to be

$$j_{\rm sync}(\nu, r, z) = \int_{m_e}^{M_\chi} dE \left(\frac{dn_{\rm e^-}}{dE} + \frac{dn_{\rm e^+}}{dE}\right) P_{\rm sync}(\nu, E, r, z) \tag{4}$$

The factor $\frac{dn_e}{dE}$ describes the particle (electron and positron respectively) equilibrium distribution. When considering dark matter induced radio emission the diffusion and energy loss experienced by the resultant electrons must be considered. This is due to the fact that position and energy distributions of the electrons will influence the subsequent synchrotron emission [20]. The equilibrium distributions can be found by solving the diffusion-loss equation under the assumption of vanishing time derivatives.

$$0 = \frac{\partial}{\partial t}\frac{dn_e}{dE} = \nabla\left(D(E,\mathbf{x})\nabla\frac{dn_e}{dE}\right) + \frac{\partial}{\partial E}\left(b(E,\mathbf{x})\frac{dn_e}{dE}\right) + Q_e(E,\mathbf{x}) \tag{5}$$

In the above equation $\frac{dn_e}{dE}$ is the electron equilibrium distribution, the spatial diffusion is described with $D(E,\mathbf{x})$, $b(E,\mathbf{x})$ describes the rate of energy loss and the electron source function is given by the function $Q_e(E,\mathbf{x})$. The per annihilation electron yield function for the 2HDM+S channel can be found in [22]. For the other annihilation channels see [23]. Typical methods for solving the diffusion equation are outlined in [20]. The Green's function method is used in this work. The flux density spectrum within a radius r of the halo centre is then found to be

$$S_{\mathrm{sync}}(\nu,z) = \int_0^r d^3r' \frac{j_{\mathrm{sync}}(\nu,r',z)}{4\pi D_L^2} \tag{6}$$

where D_L is the luminosity distance to the source in question [20].

4. MGCLS

Galaxy clusters are the largest gravitationally bound structures in their universe. The matter budget within them is dominated by dark matter. This makes them promising astrophysical laboratories for the search for potential dark matter signatures. A fraction of clusters contain a detectable diffuse radio source. This component can be used to place constrains on a dark matter model, by comparing the measured values to predictions. Observational data indicates that the spectrum of the emission is steep (see reviews [24],[25]). This information can potentially be used to probe the distributions of the cosmic ray particles as well as the cluster magnetic fields [9]. More accurate representations of cluster magnetic fields will reduce the uncertainties of the modelled dark matter signals. In turn this could lead to more reliable constraints on the dark matter properties within the test model. As found in this study and others [26], a limited number of clusters have well studied magnetic fields. Thus MeerKAT's potential for studying magnetic fields may greatly benefit attempts at constraining dark matter. The data used in this work is obtained from the MeerKAT Galaxy Cluster Legacy Survey (MGCLS). Detailed information of MGCLS can be found in Knowles et al [9]. The procedure used to obtain the integrated fluxes of the radio halos is outlined in [10]. The use of the SAODS9 radio flux measurement is acknowledged [27].

5. Results and Discussion

The sample size of clusters investigated in this work is twelve. For seven clusters the virial mass and radius was found in literature. This information was used to simulate the halo environments. These properties are listed in Table 1. For the remaining clusters the only available mass information found was M_{500}. From this information the characteristic density and scale radius can be found. This is done by solving

$$\int_0^{\mathrm{r_{500}}} \rho(r) 4\pi r^2 dr = \mathrm{M_{500}} \tag{7}$$

and

$$\int_0^{r_{500}} \rho(r)dr = 500\rho_c \frac{4\pi r_{500}^3}{3} \tag{8}$$

simultaneously by assuming the NFW density profile

$$\rho(r) = \frac{\rho_0}{\frac{r}{r_s}(1+\frac{r}{r_s})} \tag{9}$$

The modelled signals consider that the dark matter distribution is smooth. It is known that physical halos have a more clumpy distribution due to the presence of substructure as predicted through the bottom-up formation model. The more concentrated regions are expected to enhance the signal [28, 29]. This is due to the signal's proportionality to the square of the density. The boost effect is more enhanced in larger halos, as they contain more hierarchical levels of structure formation.The total halo boost factors can be calculated using the parametric equation in [29] with α=2. For the masses of the clusters considered the total boost factor is approximately 60. However this factor is produced mainly for a γ-ray signal. Synchrotron emissions will not experience this full boost factor, as sub-halos are more common around the outskirts of the host halo. In these regions the magnetic fields are generally much weaker. Thus it is necessary to calculate a scaled boost factor. This can be accomplished by multiplying the distribution of the host halo with a modification function from [30] in order to obtain the mass distribution of the sub-halos. This density is then normalized to produce a probability distribution. The scaled boost factor is then the sub over the probability of a sub-halo being at the given radius multiplied by the magnetic scaling factor at that point.

Table 1: Physical characteristics of the clusters. Column 2: redshift. Column 3: virial mass. Column 4: halo scale radius- defined as the virial radius divided by the virial concentration. Common alternate names are provided in column 5 and the scaled boost factor is given in column 6.

Cluster name	z	M_{vir} (10^{15} $M_\odot$)	R_s (Mpc)	Alternate name	Scaled Boost	References
Abell 209	0.206	1.35	0.62		5.69	[9] [31]
Abell 370	0.375	3.03	0.36	G172.98-53.55	5.78	[9] [32] [33]
Abell 2813	0.29	1.241	0.61	J0043.4-2037	2.84	[9] [31]
Abell S295	0.3	0.51	0.44	J0245.4-5302	5.58	[9] [31]
Abell S1063	0.348	1.49	0.66	J2248.7-4431	5.74	[9] [31]
J0528.9-3927	0.284	1.64	0.65		1.82	[9] [34]
J0645.4-5413	0.167	1.24	0.61	Abell 3404	4.27	[9] [31]

Table 2: Physical characteristics of the clusters. Column 2: redshift. Column 3: characteristic density. Column 4: halo scale radius. Common alternate names are provided in column 5 and the scaled boost factor is given in column 6.

Cluster name	z	ρ_s (10^{14} $M_\odot$/Mpc)	R_s (Mpc)	Alternate name	Scaled Boost	References
Abell 545	0.154	1.23	0.99	J0532.3-1131	2.24	[9] [35]
Abell 2667	0.230	2.91	0.89	J2351.6-2605	1.08	[9] [36]
J0303.7-7752	0.274	2.97	0.8	G294.66-37.02	2.57	[9] [36]
J0638.7-5358	0.233	3.86	0.82	Abell S592	2.76	[9] [36]
J1601.7-7544	0.153	3.46	0.76	G313.88-17.12	1.78	[9] [36]

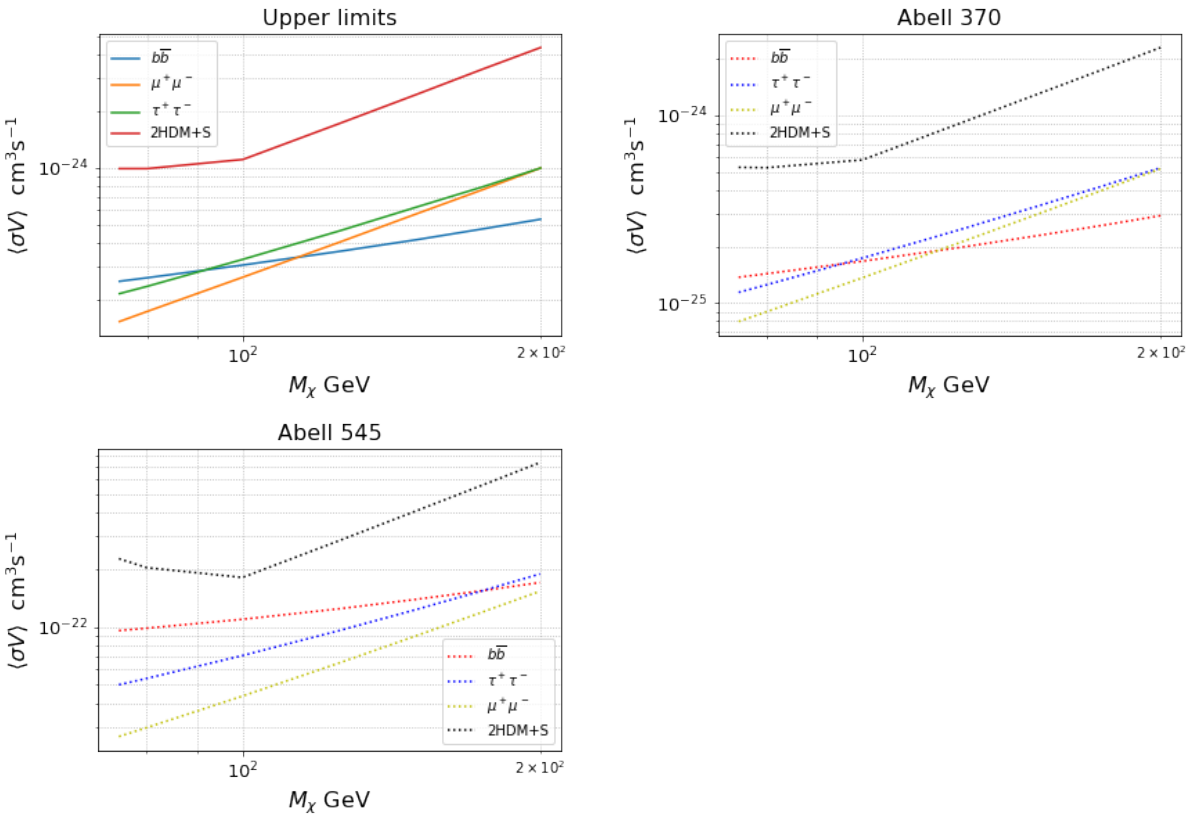

Figure 1: Annihilation rates at a 2σ confidence level for the annihilation channels over the mass range 75-200 GeV. The statistically stacked results are dominated by the most constraining results A370, but are slightly skewed by other underperforming clusters such as A545.

The mass range that has been considered is 75-200 GeV in order to overlap with the mass range of the 2HDM+S dark matter candidate expected from kinematic considerations [3], and fitting to the astrophysical excesses. The simulated fluxes are compared to the measured values with a 2σ confidence level. The error in the measured value is estimated with a sum of squares value of a 5% systematic error due to the calibration of the equipment as well a statistical error given by SAODS9 in the flux measurement. The results of the twelve individual clusters are stacked. The tightest constraints arise from Abell 370, the largest and most distant cluster. The least constraining results are found in Abell 545, one of the closest and smallest clusters. The remaining results lie between these two ends.

The cross section limits produced are above the thermal relic value, $\langle\sigma V\rangle \approx 10^{-26}$. Thus the dark matter model can not be ruled out as a candidate for all dark matter, as its present abundance may be less than what is required to agree with present cosmological constraints. Future work will consider the cases of faint mini halos as well as non-detection of diffuse emission. This will lower the surface brightness values that the dark matter signal will be constrained by.

Acknowledgments
N.L acknowledges the financial assistance of the South African Radio Observatory (SARAO) towards this research (www.sarao.ac.za).

[1] Bertone G, Hooper D and Silk J 2005 *Physics reports* **405** 279–390

[2] Von Buddenbrock S, Chakrabarty N, Cornell A S, Kar D, Kumar M, Mandal T, Mellado B, Mukhopadhyaya B and Reed R G 2015 *arXiv preprint arXiv:1506.00612*
[3] von Buddenbrock S, Chakrabarty N, Cornell A S, Kar D, Kumar M, Mandal T, Mellado B, Mukhopadhyaya B, Reed R G and Ruan X 2016 *The European Physical Journal C* **76** 1–18
[4] Picozza P, Galper A, Castellini G, Adriani O, Altamura F, Ambriola M, Barbarino G, Basili A, Bazilevskaja G, Bencardino R *et al.* 2007 *Astroparticle physics* **27** 296–315
[5] Fermi-LAT https://fermi.gsfc.nasa.gov/ ,(Accessed 2021-03-24)
[6] Atwood W, Abdo A A, Ackermann M, Althouse W, Anderson B, Axelsson M, Baldini L, Ballet J, Band D, Barbiellini G *et al.* 2009 *The Astrophysical Journal* **697** 1071
[7] Foo H.E.S.S https://www.mpi-hd.mpg.de/hfm/HESS/, (Accessed 2021-03-01)
[8] Chan M H 2021 *Galaxies* **9** 11
[9] Knowles K, Cotton W, Rudnick L, Camilo F, Goedhart S, Deane R, Ramatsoku M, Bietenholz M, Brüggen M, Button C *et al.* 2022 *Astronomy & Astrophysics* **657** A56
[10] Lavis N and Beck G 2022 *arXiv preprint arXiv:2208:06813*
[11] Higgs P W 1964 *Physical Review Letters* **13** 508
[12] Higgs P W 1964 *Phys. Lett.* **12** 132–133
[13] Englert F and Brout R 1964 *Physical review letters* **13** 321
[14] Guralnik G S, Hagen C R and Kibble T W 1964 *Physical Review Letters* **13** 585
[15] Von Buddenbrock S, Cornell A S, Mohammed A F, Kumar M, Mellado B and Ruan X 2018 *Journal of Physics G: Nuclear and Particle Physics* **45** 115003
[16] von Buddenbrock S, Cornell A S, Fang Y, Mohammed A F, Kumar M, Mellado B and Tomiwa K G 2019 *Journal of High Energy Physics* **2019** 1–41
[17] von Buddenbrock S, Ruiz R and Mellado B 2020 *Physics Letters B* **811** 135964
[18] Hernandez Y, Kumar M, Cornell A S, Dahbi S E, Fang Y, Lieberman B, Mellado B, Monnakgotla K, Ruan X and Xin S 2021 *The European Physical Journal C* **81** 1–13
[19] Crivellin A, Fang Y, Fischer O, Kumar A, Kumar M, Malwa E, Mellado B, Rapheeha N, Ruan X and Sha Q 2021 *arXiv preprint arXiv:2109.02650*
[20] Beck G 2019 *Galaxies* **7** 16
[21] Longair M S 2010 *High energy astrophysics* (Cambridge university press)
[22] Beck G, Kumar M, Malwa E, Mellado B and Temo R 2021 *arXiv preprint arXiv:2102.10596*
[23] Cirelli M, Corcella G, Hektor A, Hütsi G, Kadastik M, Panci P, Raidal M, Sala F and Strumia A 2011 *Journal of Cosmology and Astroparticle Physics* **2011** 051
[24] Feretti L, Giovannini G, Govoni F and Murgia M 2012 *The Astronomy and Astrophysics Review* **20** 1–60
[25] Van Weeren R, de Gasperin F, Akamatsu H, Brüggen M, Feretti L, Kang H, Stroe A and Zandanel F 2019 *Space Science Reviews* **215** 1–75
[26] Storm E, Jeltema T E, Profumo S and Rudnick L 2013 *The Astrophysical Journal* **768** 106
[27] SAODS9- radio flux measurements
[28] Sánchez-Conde M A and Prada F 2014 *Monthly Notices of the Royal Astronomical Society* **442** 2271–2277
[29] Moliné Á, Sánchez-Conde M A, Palomares-Ruiz S and Prada F 2017 *Monthly Notices of the Royal Astronomical Society* **466** 4974–4990
[30] Jiang F and van den Bosch F C 2017 *Monthly Notices of the Royal Astronomical Society* **472** 657–674
[31] Klein M, Israel H, Nagarajan A, Bertoldi F, Pacaud F, Lee A T, Sommer M and Basu K 2019 *Monthly Notices of the Royal Astronomical Society* **488** 1704–1727
[32] Lee J H, Kang J, Lee M G and Jang I S 2020 *The Astrophysical Journal* **894** 75
[33] Bartelmann M 1996 *arXiv preprint astro-ph/9602053*
[34] Foëx G, Chon G and Böhringer H 2017 *Astronomy & Astrophysics* **601** A145
[35] Mantz A B, Allen S W, Morris R G, von der Linden A, Applegate D E, Kelly P L, Burke D L, Donovan D and Ebeling H 2016 *Monthly Notices of the Royal Astronomical Society* **463** 3582–3603
[36] Rossetti M, Gastaldello F, Eckert D, Della Torre M, Pantiri G, Cazzoletti P and Molendi S 2017 *Monthly Notices of the Royal Astronomical Society* **468** 1917–1930